Anisotropic Ballistic Transport Revealed by Molecular Nanoprobe Experiments

Markus Leisegang,[1,*] Robert Schindhelm,[1] Jens Kügel,[1] and Matthias Bode[1,2]
[1]Physikalisches Institut, Experimentelle Physik II, Universität Würzburg, Am Hubland, 97074 Würzburg, Germany
[2]Wilhelm Conrad Röntgen-Center for Complex Material Systems (RCCM), Universität Würzburg, Am Hubland, D-97074 Würzburg, Germany

(Received 4 October 2020; revised 27 February 2021; accepted 15 March 2021; published 7 April 2021)

Atomic-scale charge transport properties are not only of significant fundamental interest but also highly relevant for numerous technical applications. However, experimental methods that are capable of detecting charge transport at the relevant single-digit nanometer length scale are scarce. Here we report on molecular nanoprobe experiments on Pd(110), where we use the charge carrier-driven switching of a single cis-2-butene molecule to detect ballistic transport properties over length scales of a few nanometers. Our data demonstrate a striking angular dependence with a dip in the charge transport along the $[1\bar{1}0]$-oriented atomic rows and a peak in the transverse [001] direction. The narrow angular width of both features and distance-dependent measurements suggest that the nanometer-scale ballistic transport properties of metallic surfaces are significantly influenced by the atomic structure.

DOI: 10.1103/PhysRevLett.126.146601

Introduction.—The fate of elementary charges injected into a surface or interface is of fundamental interest for a myriad of technical applications. Because of their importance in CMOS transistors [1–3] and photovoltaics [4–7], ballistic hot electrons and holes, i.e., charge carriers with an energy well above the thermally broadened Fermi level, have attracted particular attention. Immediately upon injection, ballistic charge carriers occupy an intermediate state, the properties of which are determined by the specific band structure of the receiving electrode [8]. The dispersion relation of this band initially also dictates charge carrier propagation until, after a few femtoseconds, a sequence of multiple weakly inelastic scattering events sets in. These events drive it toward the band bottom and result in a quasithermal equilibrium where diffusive transport dominates [8].

Since the building blocks of current electronics products often rely on functionalities where the atomic structure plays an important role, the investigation of ballistic transport on atomic length scales, where the interaction of charge carriers with single discontinuities could be investigated, would be highly beneficial. Conventional (single-tip) STM and spectroscopy allow for the imaging of the surface structure and local density of states with atomic spatial resolution, respectively. However, ballistic transport properties can only be probed to a limited extent by the quasiparticle interference technique because the tip simultaneously serves to inject and detect the charge carriers. As a result, the quasiparticle interference is restricted to transport pathways that exhibit a closed loop.

To overcome this limitation, several two-probe (2P) or even multiple-probe STMs have been designed, built, and used [9–12]. A recent study demonstrated [13] that the high stability of cryogenic setups allows one to position two tips of a 2P STM on the same dimer row of a $\mathrm{Ge}(001)$-$\mathrm{c}(4\times 2)$ surface. By driving a charge current through the intermediate sample, it became possible to observe one-dimensional ballistic transport down to an interprobe distance $d_{\mathrm{pp}} = 30$ nm [13]. Even shorter distances are impeded by the spatial extent of the two probe tips, which, with good approximation, can be assumed to be spherical with a typical diameter of 20 to 40 nm [11].

In an alternative approach, charge currents injected by the tip of a conventional one-probe STM may be detected by molecular reactions [14–17]. Now the diameter of the one STM tip is no longer a limiting factor. Reversible switching of a single molecule is used in the so-called molecular nanoprobe (MONA) technique, which allows for transport studies down to few atom length scales [18–21]. Furthermore, this technique allows one to arbitrarily position the tip with respect to the detector molecule, whereas the shafts of the two probe tips in 2P STM experiments may inhibit some configurations. This opens up the opportunity to investigate if and to what extent the atomic lattice of highly anisotropic surfaces impacts their transport properties.

In this Letter, we report on MONA experiments performed on the (110) surface of face-centered cubic Pd. Using a single cis-2-butene as a detector molecule, we investigate the ballistic transport of charge carriers that are injected by an STM tip at probe-molecule distances of a few nanometers only. Our experimental data demonstrate a striking angular dependence. In particular, we observe a dip in the charge transport along the $[1\bar{1}0]$-oriented atomic rows and a peak in the transverse [001] direction. The narrow angular width of both features and results obtained in

distance-dependent measurements suggest that the nanometer-scale charge transport properties of metallic surfaces are significantly influenced by the atomic structure.

Experimental setup.—Experiments were performed in a low-temperature STM at temperature $T \approx 4.5$ K. The Pd (110) surface was prepared by cycles of Ar^+ sputtering with an ion energy of 0.7 keV and subsequent annealing at 780 K for 20 min. The cleanliness of the Pd(110) surface region for subsequent measurements is verified by an initial topographic scan before dosing minute amounts of cis-2-butene onto the surface inside the low-temperature STM at cryogenic temperatures.

Results.—Figure 1(a) shows a constant-current STM image of a single cis-2-butene molecule (c2b) adsorbed on Pd(110). The substrate's atomic distance along the [001] direction is a factor of $\sqrt{2}$ larger than along the $[1\bar{1}0]$ direction. This structural anisotropy of Pd(110) leads to a striped appearance in STM images, with adjacent $[1\bar{1}0]$-oriented atomic rows being separated by 389 pm. The inset in Fig. 1(a) indicates the adsorption geometry of c2b on top of two neighboring atoms of a densely packed Pd row [22]. When imaged by STM, the c2b appears in an avocado shape, where the enlarged bright end depicts the two end-standing carbon atoms and the elongated tail corresponds to the center carbon atoms enclosing the double bond.

As first reported in Ref. [23] and confirmed by us, charge currents between the STM tip and the substrate through c2b can trigger two distinct transformations. At a bias voltage

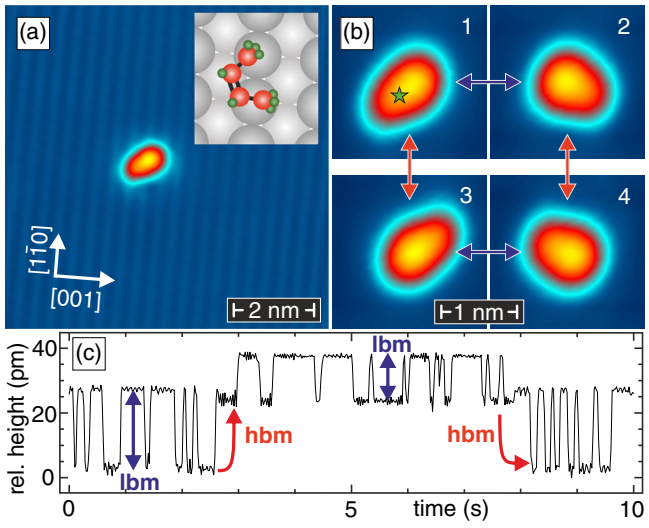

FIG. 1. (a) Topographic STM image of a single cis-2-butene (c2b) molecule on the row-wise structure of a clean Pd(110) surface. The inset schematically shows the molecule's adsorption geometry on top of a densely packed Pd row. (b) STM images of the four rotational states of c2b, labeled 1–4 (scan parameters: $U = 10$ mV; $I = 20$ pA). Blue arrows mark a low barrier motion (lbm), whereas red arrows mark a high barrier motion (hbm). (c) Telegraph noise recorded with the tip positioned at the green star in (b). Tunneling parameters: $U_{\mathrm{bias}} = 150$ mV; $I = 20$ pA.

$U_{\mathrm{lbm}} \approx 30$ mV, a reversible rotation sets in that converts the molecule into its mirror image with respect to the $[1\bar{1}0]$ axis, as marked by blue arrows in Fig. 1(b). Owing to its low threshold energy, this transition has been called low barrier motion (lbm) [23]. At $U_{\mathrm{hbm}} \geq 100$ mV, another transition is observed that leads to a point inversion of the c2b molecule, denoted as high barrier motion (hbm) hereafter. Within our measurement accuracy, the inversion point coincides with the point of maximum corrugation, probably representing the molecule binding site. Earlier experiments showed that both excitations are induced by inelastic electron tunneling [23]. A detailed analysis revealed that the hbm is mainly driven by the C = C stretch mode, whereas the lbm is related to the Pd–C stretch mode.

These reversible transitions result in four molecular adsorption geometries, labeled as states 1 to 4 in Fig. 1(b). When choosing a suitable tip position where the four states are distinguishable, such as the one marked by a green star in Fig. 1(b), we can determine the actual state of the molecule by recording the tip height. An example of the resulting telegraph noise is shown in Fig. 1(c). For $t \lesssim 2.6$ s, the apparent height fluctuates by about 25 pm, indicating lbm between states 1 and 2. Then, a more rare hbm to the high levels representing states 3 and 4 occurs, followed by lbm between these two states. Finally, at $t \approx 7.9$ s another hbm sets the molecule back to states 1 and 2. Our observations are in full accordance with previous findings reported in Ref. [23].

All data presented so far were measured with the STM tip positioned on top of the molecule. In order to investigate if the anisotropic structure of the Pd(110) surface also influences its charge transport properties in the ballistic regime, we conducted measurements with the MONA technique [20]. In short, MONA uses a charge carrier-driven molecular switching event, such as a tautomerization or rotation, to detect currents injected a few nanometers away. Since the activation barrier of the molecular rotation essentially represents a high pass filter of the detection process, only the ballistic charge carrier, in this case with the threshold energy of the lbm, $eU_{\mathrm{lbm}} > 30$ meV, can be detected. In this Letter, we show that, by placing the STM tip and thereby the charge carrier injection point at different locations relative to the detector molecule, the influence of an anisotropic atomic lattice on ballistic transport can be evaluated. The measurement procedure is based on the cyclical repetition of three steps. First (i), the initial state of the molecule is probed by a topographic scan at noninvasive parameters ($U = 10$ mV, $I = 20$ pA). Then (ii), the tip is moved to the excitation position at a distance r from the detector molecule and charge carriers are injected at excitation parameters $U_{\mathrm{exc}} = -50$ mV and $I_{\mathrm{exc}} = 8$ nA. Eventually (iii), the final state of the c2b molecule is probed by another topographic scan at noninvasive parameters. Switching events between the rotational states are detected by comparing the STM images before and after each

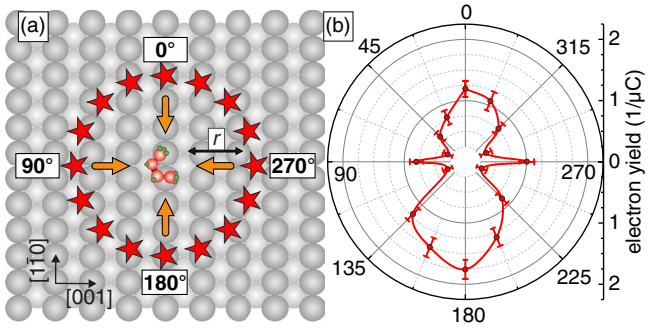

FIG. 2. (a) Schematic representation of the MONA measurements conducted to detect the direction-dependent transport properties of the Pd(110) surface. Sixteen injection points, marked by red stars, are equidistantly arranged on a circle with radius $r = 3$ nm around a single cis-2-butene molecule, resulting in an angular resolution $\Delta\varphi = 22.5°$. Gray spheres represent the surface atomic structure of Pd(110) (not in scale). (b) Polar plot showing the excitation angle-dependent electron yield (excitation parameters: $U_{exc} = -50$ mV, $I_{exc} = 8$ nA, $t_{exc} = 8$ s). The line serves as a guide for the eye only.

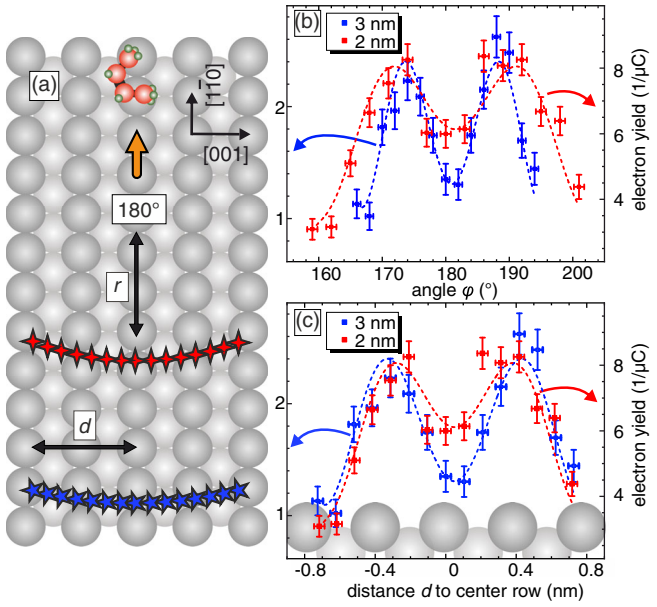

FIG. 3. (a) Measurement scheme of transport measurements performed around the [1$\bar{1}$0] direction at distances of $r = 2$ nm (red) and 3 nm (blue) to the detector molecule. (b) Plot of the electron yield as a function of the angle θ relative to the [1$\bar{1}$0] direction. (c) Plot of the electron yield as a function of the distance d of the injection point from the adatom row where the c2b detector molecule is adsorbed (excitation parameters: $U_{exc} = -50$ mV; $I_{exc} = 8$ nA, $t_{exc} = 8$ s). A narrow minimum located at the central row, which is surrounded by a symmetric double peak structure, can be recognized.

injection. The switching probability is obtained by calculating the average of numerous measurements. To avoid the excitation of two or more switching processes with a single pulse, the probability per pulse is kept well below 15%. The statistical standard variation of every data point presented in this work represents a minimum of 600 repetition cycles. Finally, we calculated the total electron yield η by dividing the observed number of switching events N_{sw} through the amount of injected charge N_{el}. The error bar for a calculated electron yield is given by $\Delta\eta = \sqrt{[\eta(1-\eta)]/N_{el}}$.

In a first set of direction-dependent measurements, the switching rate of a single c2b molecule was investigated by injecting charge carriers at a constant distance of $r = 3$ nm from the molecule center under variations of the azimuthal angle. The 16 excitation positions are represented as red stars in Fig. 2(a), which for comparison also shows the surface atomic structure of Pd(110) (not in scale). As indicated by orange arrows, measurements performed at 0° and 180° probe the transport properties along the [1$\bar{1}$0]-oriented atomic rows of the Pd(110) surface, whereas data obtained at 90° and 270° give access to the transverse [001] direction. The results are shown in polar coordinates in Fig. 2(b). On a qualitative level, we recognize a pronounced anisotropy with two main features: (i) Most apparent are broad maxima at 0° and 180°, where the electron yield is four to six times higher than in the minima around 90° and 270°. Furthermore, (ii) the data exhibit more narrow maxima at 90° and 270°, which are not as high as the values observed at 0° and 180° but still exceed the surrounding minima by roughly a factor of 3 [24].

To shed light on the question of whether the striking anisotropy observed in Fig. 2 is driven by the dispersion relation or by scattering on single atomic rows, we performed MONA measurements at refined angle resolutions. The data obtained around the [1$\bar{1}$0] direction are presented in Fig. 3. As sketched in Fig. 3(a), we took two sets of data at tip-molecule distances of $r = 2$ nm (red stars) and $r = 3$ nm (blue). In both cases, 15 equidistant data points were taken, resulting in angular resolutions of $\Delta\varphi = 3°$ and 2°, respectively. A comparison to the surface lattice, which is represented as true-to-scale spheres in Fig. 3(a), shows that the spacing of data points is well below the interrow distance.

Figures 3(b) and 3(c) show the measured electron yield plotted versus the angle ϕ and the distance from the central densely packed Pd row d, respectively. Based on the results obtained at low angular resolution in Fig. 2(b), the findings presented here are quite surprising. Instead of a broad peak we now, at a much better resolution, recognize a narrow minimum located on the central row that is surrounded by a symmetric double peak structure. Comparing Fig. 3(b) and 3(c) reveals that the data coincide significantly better in the representation over the distance d. Therefore, we conclude that the absolute charge carrier injection position on the row-wise structure rather than the relative direction of the charge carrier propagation is relevant for the transport.

The observation of this narrow minimum suggests that the [1$\bar{1}$0]-oriented adatom rows posses a resistance that is

enhanced compared to the troughs in between. Moving the charge carrier injection point away from this row through the intermediate trough to the next adatom rows leads to an enhanced transport as detected by an increasing electron yield. Only if the tip is moved further sideways beyond this adjacent adatom row a steep decline in the measured electron yield is detected.

In a second set of measurements with subatomic resolution, we investigated the charge carrier transport along the [001] direction, i.e., transverse to the atomic rows. As marked by red stars in Fig. 4(a), we chose 16 equidistant excitation points at distances r in the range between $r = 2$ nm and $r = 3.5$ nm from the molecular center. The respective electron yields are shown in Fig. 4(b). The distance r dependence of the ballistic transport current I_b can be described by $I_b = r^{-n} \cdot \exp(-r/L_{inel})$, where the first term depicts the intensity decay in $n + 1$ dimensions and the second term describes the exponential damping due to inelastic scattering on the characteristic length scale L_{inel}. Fitting the data to 1D, 2D, and 3D transports results in very similar values of 0.5 nm $< L_{inel} <$ 1 nm, represented by dashed lines in Fig. 4(b). This value is much lower than the inelastic mean free path (IMFP) usually found for very low electron energy, e.g., in noble metals [25], and might be caused by enhanced d-band scattering in Pd [26], which also inhibits the unambiguous identification of the dimension of the transport channel.

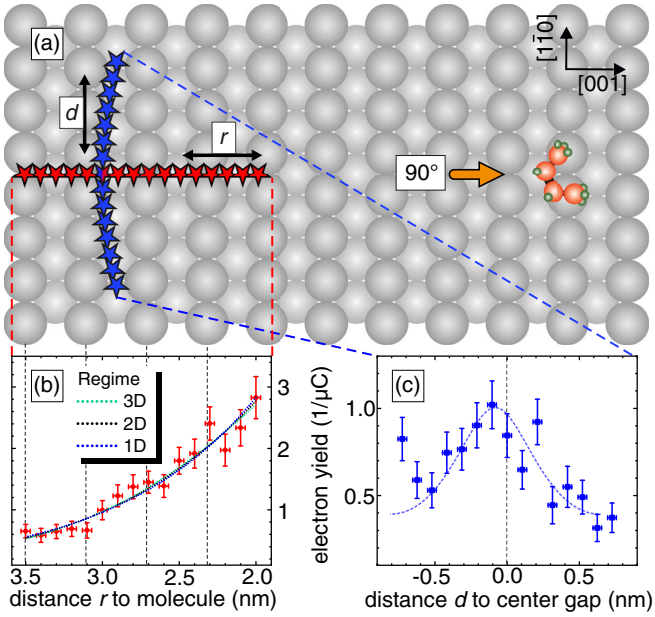

FIG. 4. (a) Scheme of MONA measurements performed to determine the distance dependence (red stars) and angular dependence around the [001] direction (blue). (b) Plot of the distance-dependent electron yield for 2 nm $\leq r \leq$ 3.5 nm with fits for 1D, 2D, and 3D ballistic transport regimes. (c) Electron yield as a function of the distance d of the injection point from the center gap row where the molecule c2b detector molecule is adsorbed. Excitation parameters: $U_{exc} = -50$ mV; $I_{exc} = 8$ nA, $t_{exc} = 8$ s.

A complementary series of measurements was taken at 15 points around 90° along a circular arc with a radius of $r = 3$ nm—see blue stars in Fig. 4(a)—granting an angular resolution $\Delta\varphi = 2°$. The resulting electron yield is displayed in Fig. 4(c). We recognize a peak around the central atomic gap $d = 0$ nm, which quickly drops as the injection point is moved away from this position. Analysis reveals a peak width equivalent to the molecular adsorption site of about two atoms [27].

Discussion.—The MONA data presented in Figs. 2–4 unambiguously show that ballistic charge carrier transport on Pd(110) surfaces is strongly anisotropic. Measurements performed at relatively low angular resolutions reveal that electron transport is more efficient along the [1$\bar{1}$0] direction compared to the [001] direction. This anisotropy might, in principle, be caused either by potential wells formed by the adatom rows or by an anisotropic band structure of the Pd (110) surface or by a combination of both effects. High angular resolution measurements reveal two very narrow features along the high symmetry directions, i.e., a double peak in the [1$\bar{1}$0] direction and a single peak along [001]. The data presented in Figs. 3 and 4 evidence that the width of both features correlate much better to the real space atomic lattice than the angle under which the charge injection is performed. These observations indicate that the adatoms, which create a row-wise structure on face-centered cubic (110) metal surfaces, serve as scattering potentials for the ballistic transport of hot charge carriers and that the band structure is of secondary relevance.

We speculate that the LDOS of the d-derived bands responsible for the unusual short IMFP of Pd [26] accumulates at the adatom rows along the [1$\bar{1}$0] direction and decreases between them. This enhanced d LDOS would lead to a potential welllike periodic variation of the electrostatic potential $V(r)$ with a high potential and strong scattering on top of the rows and potential troughs with much weaker scattering in between. Indeed, density functional theory calculations performed for Cu(110) also revealed a similar effect that results in a $V(r)$ modulation of a few hundred meV [28]. As a result of this potential landscape, we measure a relatively low electron yield when the tip and the molecule are positioned on the same adatom row, since many electrons are scattered inelastically on their way from the injection point to the detector molecule. The assumption of scattering centers aligned along the adatom rows is also corroborated by the clear difference between the electron yield measure at $d = 0$ nm for $r = 2$ nm and $r = 3$ nm, cf. Fig. 3(c). For $r = 3$ nm, we recognize a deeper minimum, indicating that the larger number of scatterers present along the longer path results in a stronger reduction of the transport. Moving the tip away from the center row to the adjacent trough reduces scattering and results in an increased transport toward the molecule and,

thereby, an increased electron yield. Only if the injection point is moved across the next adatom row does its additional scattering potentials become effective, resulting in a strong decline of the transport.

Experiments along the [001] direction further underpin the assumption of strongly localized scattering potentials. On the one hand, we find that the IMFP of the charge carriers is on the order of one nanometer only, much shorter than what is usually observed for other noble metals. According to Ref. [26], the extraordinary reduction of the IMFP in Pd is caused by the strong contribution of d bands at the Fermi level. On the other hand the data presented in Fig. 4(c) reveal that scattering is reduced for charge carriers that propagate exactly perpendicularly to densely packed rows, as indicated by the higher electron yield. Therefore, we conclude that the row-wise atomic structure and the related surface potential is the main factor that determines the transport properties of the Pd(110) surface. However, we cannot exclude that the anisotropic band structure also has some effect, though much weaker.

In summary, our results show that the charge carrier-induced switching of a single cis-2-butene molecule can be used to detect the ballistic transport properties of Pd(110) on length scales of a few nanometers. We find a rich structure with two sharp features, i.e., a dip along the $[1\bar{1}0]$-oriented atomic rows and a peak in the [001] direction. These measurements provide evidence that the nanometer-scale charge transport properties of metallic surfaces is significantly influenced by scattering events on the atomic structure. We envision that similar measurements performed on materials more relevant for applications may not only lead to a better understanding of ballistic transport on atomic length scales but could also help in optimizing the performance of nanoscale contacts and electrical junctions.

We would like to thank S. Heinze and S. Haldar (Univ. Kiel) for insightful discussions. We acknowledge financial support by the Deutsche Forschungsgemeinschaft (DFG, German Research Foundation) through Grant No. BO 1468/27-1 and under Germany's Excellence Strategy through Würzburg–Dresden Cluster of Excellence on Complexity and Topology in Quantum Matter ct.qmat (EXC 2147, project-id 390858490).

*Corresponding author.
markus.leisegang@physik.uni-wuerzburg.de

[1] V. Sverdlov, E. Ungersboeck, H. Kosina, and S. Selberherr, Current transport models for nanoscale semiconductor devices, Mater. Sci. Eng. Rep. **58**, 228 (2008).

[2] G. Tagliabue, J. S. DuChene, A. Habib, R. Sundararaman, and H. A. Atwater, Hot-hole versus hot-electron transport at Cu/GaN heterojunction interfaces, ACS Nano **14**, 5788 (2020).

[3] P. Duhan, V. R. Rao, and N. R. Mohapatra, Effect of device dimensions, layout and pre-gate carbon implant on hot carrier induced degradation in HKMG nMOS transistors, IEEE Trans. Device Mater. Reliab. **20**, 555 (2020).

[4] N. M. Gabor, J. C. W. Song, Q. Ma, N. L. Nair, T. Taychatanapat, K. Watanabe, T. Taniguchi, L. S. Levitov, and P. Jarillo-Herrero, Hot carrier–assisted intrinsic photoresponse in graphene, Science **334**, 648 (2011).

[5] A. A. Bakulin, A. Rao, V. G. Pavelyev, P. H. M. van Loosdrecht, M. S. Pshenichnikov, D. Niedzialek, J. Cornil, D. Beljonne, and R. H. Friend, The role of driving energy and delocalized states for charge separation in organic semiconductors, Science **335**, 1340 (2012).

[6] C. Clavero, Plasmon-induced hot-electron generation at nanoparticle/metal-oxide interfaces for photovoltaic and photocatalytic devices, Nat. Photonics **8**, 95 (2014).

[7] A. M. Burger, R. Agarwal, A. Aprelev, E. Schruba, A. Gutierrez-Perez, V. M. Fridkin, and J. E. Spanier, Direct observation of shift and ballistic photovoltaic currents, Sci. Adv. **5**, eaau5588 (2019).

[8] H. G. Etheridge, K. R. Rusimova, and P. A. Sloan, The nanometre limits of ballistic and diffusive hot-hole mediated nonlocal molecular manipulation, Nanotechnology **31**, 105401 (2020).

[9] T. Kanagawa, R. Hobara, I. Matsuda, T. Tanikawa, A. Natori, and S. Hasegawa, Anisotropy in Conductance of a Quasi-One-Dimensional Metallic Surface State Measured by a Square Micro-Four-Point Probe Method, Phys. Rev. Lett. **91**, 036805 (2003).

[10] I. Miccoli, F. Edler, H. Pfnür, and C. Tegenkamp, The 100th anniversary of the four-point probe technique: The role of probe geometries in isotropic and anisotropic systems, J. Phys. Condens. Matter **27**, 223201 (2015).

[11] J. Yang, D. Sordes, M. Kolmer, D. Martrou, and C. Joachim, Imaging, single atom contact and single atom manipulations at low temperature using the new scientaomicron LT-UHV-4 STM, Eur. Phys. J. Appl. Phys. **73**, 10702 (2016).

[12] B. Voigtländer, V. Cherepanov, S. Korte, A. Leis, D. Cuma, S. Just, and F. Lüpke, Invited review article: Multi-tip scanning tunneling microscopy: Experimental techniques and data analysis, Rev. Sci. Instrum. **89**, 101101 (2018).

[13] M. Kolmer, P. Brandimarte, J. Lis, R. Zuzak, S. Godlewski, H. Kawai, A. Garcia-Lekue, N. Lorente, T. Frederiksen, C. Joachim, D. Sanchez-Portal, and M. Szymonski, Electronic transport in planar atomic-scale structures measured by two-probe scanning tunneling spectroscopy, Nat. Commun. **10**, 1573 (2019).

[14] P. Maksymovych, D. B. Dougherty, X.-Y. Zhu, and J. T. Yates, Nonlocal Dissociative Chemistry of Adsorbed Molecules Induced by Localized Electron Injection into Metal Surfaces, Phys. Rev. Lett. **99**, 016101 (2007).

[15] P. A. Sloan, S. Sakulsermsuk, and R. E. Palmer, Nonlocal Desorption of Chlorobenzene Molecules from the Si(111)-(7 × 7) Surface by Charge Injection from the Tip of a Scanning Tunneling Microscope: Remote Control of Atomic Manipulation, Phys. Rev. Lett. **105**, 048301 (2010).

[16] J. Ladenthin, L. Grill, S. Gawinkowski, S. Liu, J. Waluk, and T. Kumagai, Hot carrier-induced tautomerization within a single porphycene molecule on Cu(111), ACS Nano **9**, 7287 (2015).

[17] V. Schendel, B. Borca, I. Pentegov, T. Michnowicz, U. Kraft, H. Klauk, P. Wahl, U. Schlickum, and K. Kern, Remotely controlled isomer selective molecular switching, Nano Lett. **16**, 93 (2016).

[18] J. Kügel, M. Leisegang, and M. Bode, Imprinting directionality into proton transfer reactions of an achiral molecule, ACS Nano **12**, 8733 (2018).

[19] J. Kügel, T. Zenger, M. Leisegang, and M. Bode, On the impact of geometrical factors on hot electron-induced tautomerization, J. Phys. Chem. C **123**, 17056 (2019).

[20] M. Leisegang, J. Kügel, L. Klein, and M. Bode, Analyzing the wave nature of hot electrons with a molecular nanoprobe, Nano Lett. **18**, 2165 (2018).

[21] M. Leisegang, M. Bode, and J. Kügel, Analyzing the influence of substituents on proton tautomerization—Comparison of tetra-tert-butyl phthalocyanine isomers, J. Phys. Chem. C **122**, 29633 (2018).

[22] Y. Sainoo, Y. Kim, T. Komeda, M. Kawai, and H. Shigekawa, Observation of cis-2-butene molecule on Pd(110) by cryogenic STM: Site determination using tunneling-current-induced rotation, Surf. Sci. **536**, L403 (2003).

[23] Y. Sainoo, Y. Kim, T. Okawa, T. Komeda, H. Shigekawa, and M. Kawai, Excitation of Molecular Vibrational Modes with Inelastic Scanning Tunneling Microscopy Processes: Examination Through Action Spectra of cis-2-butene on Pd (110), Phys. Rev. Lett. **95**, 246102 (2005).

[24] The atomic lattice presented in the background of Fig. 2(a) suggests an electron yield that is mirror symmetric with respect to the [001] and the $[1\bar{1}0]$ direction of Pd(110). Whereas the data are mirror symmetric with respect to the $[1\bar{1}0]$ direction, the broad lobe visible around 0° is less extended than around 180°. This asymmetry is caused by the fact that, for the data presented in Fig. 2(b) exclusively, switching events between states 1 and 2 connected by the lbm have been analyzed. As can be recognized in Fig. 1(b), the elongated tail of the of these states points toward the bottom edge of the STM image, thereby breaking the mirror symmetry with respect to the [001] axis.

[25] P. M. Echenique, R. Berndt, E. V. Chulkov, Th. Fauster, A. Goldmann, and U. Höfer, Decay of electronic excitations at metal surfaces, Surf. Sci. Rep. **52**, 219 (2004).

[26] F. Ladstädter, U. Hohenester, P. Puschnig, and C. Ambrosch-Draxl, First-principles calculation of hot-electron scattering in metals, Phys. Rev. B **70**, 235125 (2004).

[27] Again, the asymmetry around zero can be explained by the adsorption geometry of the molecule. Since the analysis is exclusively based on transitions between states 1 and 2, the elongation of the c2b along the $[1\bar{1}0]$ axis breaks the mirror symmetry with respect to the [001] axis.

[28] J. H. Stenlid, A. J. Johansson, and T. Brinck, The local electron attachment energy and the electrostatic potential as descriptors of surface–adsorbate interactions, Phys. Chem. Chem. Phys. **21**, 17001 (2019).